Received 14 August 2020; revised 9 September 2020; accepted 17 September 2020. Date of publication 22 September 2020; date of current version 5 October 2020.

Digital Object Identifier 10.1109/OJPEL.2020.3025632

Reduced-Order Thermal Modeling for Photovoltaic Inverters Considering Mission Profile Dynamics

ARIYA SANGWONGWANICH (Member, IEEE), HUAI WANG (Senior Member, IEEE), AND FREDE BLAABJERG (Fellow, IEEE)

Department of Energy Technology, Aalborg University, Aalborg DK-9220, Denmark

CORRESPONDING AUTHOR: ARIYA SANGWONGWANICH (e-mail: ars@et.aau.dk)

This work was supported in part by Innovation Fund Denmark through the Advanced Power Electronic Technology and Tools (APETT) project and in part by the Reliable Power Electronic-Based Power System (REPEPS) project at the Department of Energy Technology, Aalborg University as a part of the Villum Investigator Program funded by the Villum Foundation.

ABSTRACT Power devices are among the reliability-critical components in the Photovoltaic (PV) inverter, whose failures are normally related to the thermal stress. Therefore, thermal modeling is required for estimating the thermal stress of the power devices under long-term operating conditions of the PV inverter, i.e., mission profile. Unfortunately, most of the thermal models developed for the power device are not suitable for a long-term thermal stress analysis (e.g., days to months), and there is usually a trade-off between the model accuracy and the computational efficiency. To address this challenge, a reduced-order thermal model for PV inverters is proposed in this paper, where the model simplification is based on the thermal impedance characteristic and the mission profile dynamics. The modeling accuracy is evaluated by comparing the estimated thermal stress with the experimental results from a PV inverter test-bench, where daily mission profiles with various dynamics are tested. According to the results, the proposed method offers a relatively high model accuracy (similar to the full-order thermal model) while the computational efficiency is improved significantly, making it suitable for long-term thermal stress modeling applications.

INDEX TERMS IGBT, power semiconductor device, thermal modeling, thermal cycling, reliability, mission profile, Photovoltaic (PV) systems, inverters.

I. INTRODUCTION

Thermal stress is a key factor that influences the reliability and robustness of PV inverters [1]–[3]. Power devices such as Insulated-Gate Bipolar Transistor (IGBT) are among the reliability-critical components in the PV inverters, which are subjected to high thermal stress during inverter operation, and thus are prone to failure [4]. Accordingly, thermal modeling of the power devices is essential to ensure a reliable and robust operation of PV inverters, especially under real-field operating conditions, also referred to as mission profiles [5].

On one hand, the thermal model is required to ensure that the thermal stress of the power device, e.g., junction temperature, under the worst-case scenario (e.g., maximum loading condition) is still within a safe operating area of the component [6], [7]. This is to allocate a certain robust design margin of the power devices against the load variations [8]. On the other hand, the thermal model also plays an important role in the reliability assessment of the power devices (e.g., wear-out failure), where the dynamic loading from the mission profile needs to be translated into the junction temperature profile, and then applied to the lifetime prediction (e.g., through the cycle counting methods) [9]–[11]. These two thermal stress analysis aspects have gained more and more attention in the recent research in power electronics including PV inverter applications [12]–[14]. In both robustness and reliability aspects, the mission profile, which is a representation of the inverter operating condition, needs to be considered during the thermal stress analysis [15]. In PV applications, the mission profile parameters consist of the solar irradiance and ambient temperature, which have a time-span of several days to months

This work is licensed under a Creative Commons Attribution 4.0 License. For more information, see https://creativecommons.org/licenses/by/4.0/

when considering a seasonal variation of the mission profile dynamics. Therefore, a long-term thermal stress analysis is generally demanded for mission profile in PV applications, which brings a significant challenge in the thermal modeling of the power device.

Several thermal models have been developed for power electronics application, especially for the power devices, ranging from a very simplified one (e.g., based on a lumped thermal network) to a highly complex one (e.g., based on a finite-element model) [16]–[23]. However, due to the requirement of long-term simulations, most of the available thermal models cannot be easily applied to the thermal modeling of PV inverter under mission profile operation. In fact, a lumped thermal network is normally applied for the long-term thermal stress analysis of PV inverters due to its low computational burden and simple parameterization [24]–[31]. In the previous study, the lumped thermal network is either based on the full-order thermal model [24]–[28], which includes all the transient thermal impedance, or the steady-state lumped thermal model [29]–[31], which only considers the thermal resistance. While the full-order thermal model can provide a more accurate thermal stress modeling under dynamic conditions, it requires a much higher computational efforts during simulation compared to the steady-state thermal model, which could be crucial, e.g., when being used in the optimization routine. Thus, there is a trade-off between complexity and accuracy in the conventional thermal modeling approaches, limiting its efficiency [32]. Moreover, to the best knowledge of the authors, there is still lack of validation in terms of modeling accuracy, especially when comparing the simulation results against the real thermal stress from the field operation. Therefore, the uncertainty introduced by the thermal stress modeling during the robustness and reliability analysis has not been analyzed in the previous study.

Generally, model simplification is one commonly used approach to address the trade-off between the model accuracy and the computational requirement. According to the previous work in [33], the thermal model simplification method for periodic loading profile (e.g., fundamental frequency) has been proposed for Modular Multi-level Converter (MMC) application. However, this approach is not suitable for analyzing the thermal stress profile in a PV inverter, which, in most cases, is non-periodic due to the mission profile dynamics. Another model simplification technique has been proposed for power converters in Wind Turbine (WT) applications in [34]–[36], where different thermal models have been used for different time-scales of the mission profile dynamics. In those cases, a full-order thermal model is required between the junction and case of the IGBT power module (except the case when the mission profile dynamic is above a few hours). However, this model simplification technique is not suitable to be directly applied to the thermal stress analysis of PV inverters due to different dynamics of the cooling system. Depending on the cooling method (e.g., air-cooled or water-cooled systems), the time-constant of the heatsink (e.g., the required time to reach steady-state temperature) can be significantly different. In WT power converters, the water-cooled heatsink is normally used, which results in a fast thermal response of the case (and also heatsink) temperature [35], [37]. In that case, the time-constant of the water-cooled heatsink usually overlaps with the time-constant of the IGBT module thermal impedance. Therefore, most of the thermal stress dynamics of PV inverter occur within the junction and case of the IGBT power module but it can also affect the thermal stress dynamic of the case temperature as well.

In contrast, most of the PV inverters employ an air-cooled heatsink [3], which has a much longer time-constant for the thermal impedance. This means that the variation in the case temperature will have a much slower dynamic than the variation in the junction temperature when a power loss is applied. In other words, the dynamics of the two temperature variations can be separated (since the temperature between the junction and case of the IGBT power module can reach the steady-state much faster). In that case, simplification of the thermal model between the junction and case may be applicable (e.g., by simplifying its transient behavior) in PV inverter application (which will be demonstrated in this paper). Accordingly, different approaches for the model order reduction should be applied for the thermal modeling of PV inverters, where the time-constant of the IGBT power module (and also the cooling system) thermal impedance and the mission profile dynamics need to be considered together [38]. This aspect has not yet been addressed in the previous research.

In a word, the state-of-the-art solutions for thermal stress modeling in PV inverters still lack of:

- Validation of model accuracy under (real-field) mission profile operation
- Efficient thermal model simplification method for long-term (e.g., mission profile) thermal stress analysis

To address the above issues, a method to simplify the thermal model for PV inverter is proposed in this paper, where the mission profile dynamics are considered. A test-bench for PV inverter has been developed and it is discussed in Section II, where the junction temperature of the power device can be measured experimentally under real mission profile operation, and compared against simulations. In Section III, the thermal stress analysis of the PV inverter is carried out, where the impacts of time-constant of the thermal impedance and mission profile dynamics are analyzed. The conventional lumped thermal models are briefly discussed in Section IV. Afterward, the reduced-order thermal modeling approach is discussed in Section V, where the model simplifications are performed systematically based on the thermal stress analysis in Section III. The validation of the reduced-order thermal model is carried out in Section VI by comparing the estimated thermal stress with the experimental measurement. The model accuracy and the computational efficiency of the reduced-order thermal model are also benchmarked against the conventional thermal models. Finally, concluding remarks are provided in Section VII.

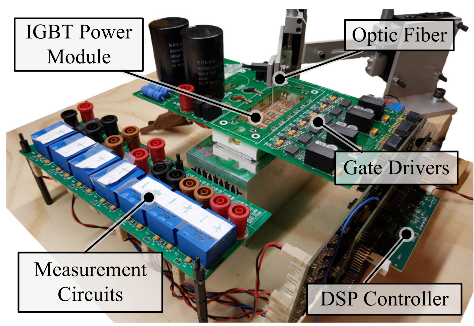

FIGURE 1. Hardware prototype of a PV inverter test-bench with the IGBT junction temperature measurement using an optic fiber.

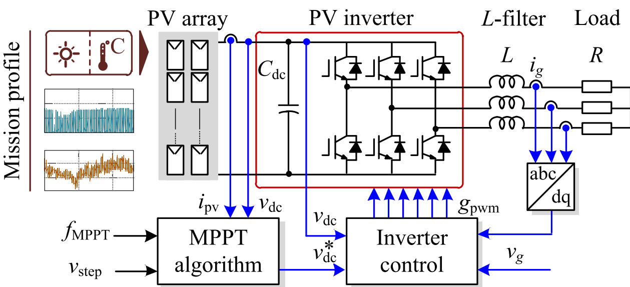

FIGURE 2. System diagram and control structure of the PV inverter test-bench.

II. TEST-BENCH FOR PHOTOVOLTAIC INVERTERS

A. SYSTEM CONFIGURATION AND CONTROL STRUCTURE

In order to validate the thermal stress modeling, a test-bench for a PV inverter, which allows an experimental measurement of power device junction temperature during mission profile operation is required. In this work, a prototype of a two-level PV inverter has been developed, where the power stage is realized by a three-phase IGBT power module, as it is shown in Fig. 1. It can be seen from the hardware prototype that the Printed Circuit Board (PCB) is custom-made, which allows direct access of the IGBT chip. During the experiments, an optic fiber is attached to the chip surface of the IGBT, as it is shown in Fig. 1. The junction temperature of the IGBT can be measured and recorded in real-time using the signal conditioner (e.g., receiver).

Besides the power stage, the test-bench consists also of a PV simulator (e.g., programmable dc power supply), output filter, and the load. The PV simulator can be programmed to emulate the electrical behavior of the PV array according to the input mission profile. Then, the MPPT algorithm is implemented in the PV inverter together with the dc-link voltage controller and current controller [39]. By doing so, a real-field mission profile operation of PV inverter can be achieved with the test-bench. The overall system diagram is illustrated in Fig. 2 and the system parameters are provided in Table 1.

B. IGBT CHARACTERIZATION

In the prototype, a 1200V/50A IGBT module [40] is used as the power stage. The characterization of the IGBT for obtaining the power losses and thermal impedance parameters will be discussed in the following.

TABLE 1 Parameters of the Three-Phase PV Inverter Test-Bench

Parameter	Value
PV array rated power	2500 W
Output current (rated)	i_g = 30 A
DC-link voltage	v_{dc} = 400-600 V
DC-link capacitance	C_{dc} = 340 μF
Filter inductance	L = 2.5 mH
Resistive load	R = 16.5 Ω
Switching frequency	f_{sw} = 10 kHz
Nominal output frequency	f_g = 50 Hz
Ambient temperature	T_a = 25 °C

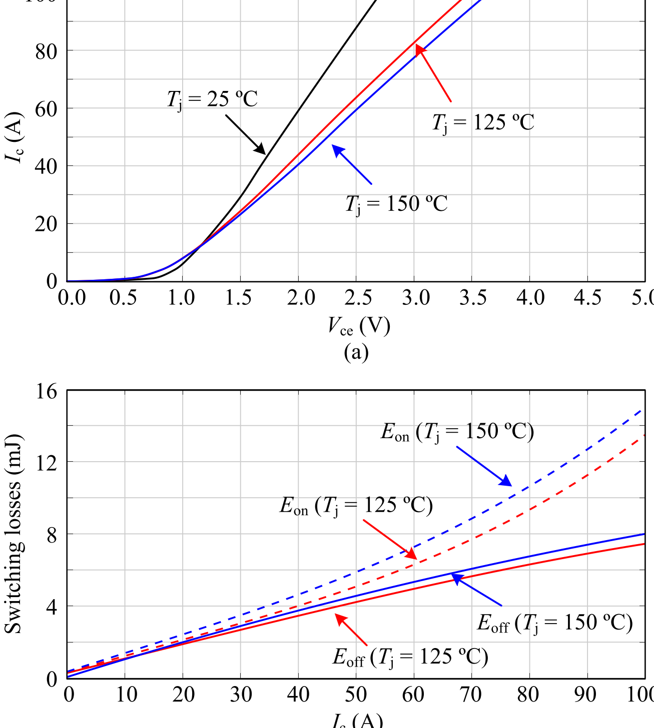

FIGURE 3. Power loss characteristic of the IGBT at different collector-emitter currents I_c and junction temperature T_j: a) Output characteristic, where V_{ce} is the on-state collector-emitter voltage and b) Switching losses, where E_{on} and E_{off} are the energy loss during turn-on and turn-off, respectively [40].

1) POWER LOSSES MODEL

Power loss of the IGBT consists of switching loss $P_{S,sw}$ and conduction loss $P_{S,con}$. In this work, a look-up table obtained from the datasheet is used for calculating the average power losses during operation (for the purpose of long-term simulation), as it is shown in Fig. 3. The total power losses dissipated in the IGBT can be obtained as given in the following:

$$P_S = P_{S,sw}(f_{sw}, E_{on}, E_{off}) + P_{S,con}(i_c, v_{ce}) \quad (1)$$

where f_{sw} is the switching frequency, E_{on} and E_{off} are the turn-on and turn-off energy, respectively, I_c and V_{ce} are the

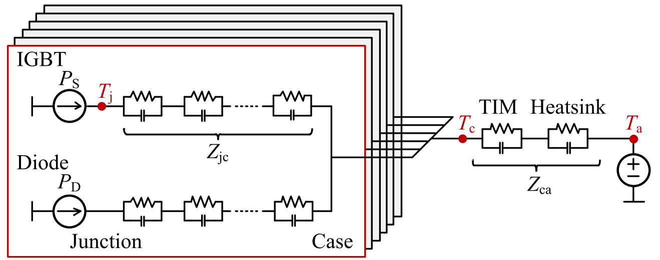

FIGURE 4. Thermal model of three-phase IGBT module in PV inverter using a (full-order) lumped thermal network.

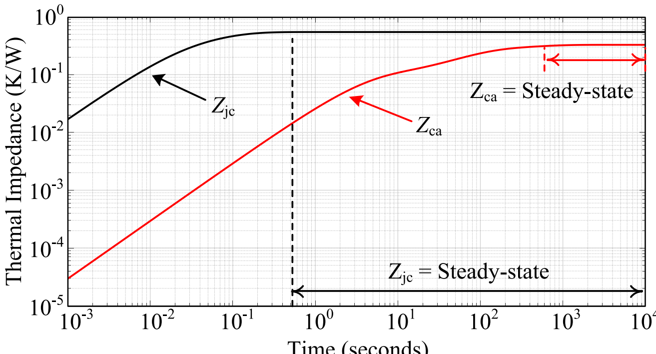

FIGURE 5. Thermal impedance of the IGBT module between junction and case Z_{jc} as well as case and ambient Z_{ca} [40].

collector-emitter current and voltage of the IGBT during conduction, respectively. Notably, the power losses are affected by the junction temperature, which is taken into account in the look-up table. The detailed power losses calculation method can be found in [41].

2) THERMAL MODEL

A thermal model of three-phase IGBT power module based on a lumped thermal network is shown in Fig. 4. There are two types of lumped thermal networks available: Cauer and Foster thermal networks. While the Cauer thermal network can represent a more physics-based thermal network, the information of the material property and geometry is normally required to calculate the model parameters, which in many cases is difficult to be obtained. On the other hand, the parameters of the Foster thermal network can be fitted from the experimental results following [37] (and also normally provided in the datasheet). Therefore, the Foster thermal network is widely used in practical applications, and it is considered in this paper.

In general, the junction temperature of the IGBT is contributed by the temperature drop inside the power module T_{jc} (e.g., between junction and case), between the case and ambient T_{ca}, and the ambient temperature T_a following:

$$\begin{aligned} T_j(t) &= T_{jc}(t) + T_{ca}(t) + T_a(t) \\ &= P_S \cdot Z_{jc}(t) + 6 \cdot (P_S + P_D) \cdot Z_{ca}(t) + T_a(t) \end{aligned} \quad (2)$$

where P_S and P_D are the total power losses of the IGBT and Diode, respectively. Z_{jc} is the thermal impedance between the junction and case of the IGBT, while Z_{ca} is the thermal impedance between the case and ambient, representing the Thermal Interface Material (TIM) and the heatsink.

According to (2), two thermal impedances Z_{jc} and Z_{ca} need to be parameterized in order to estimate the junction temperature of the IGBT for a given power loss and ambient temperature condition. The thermal impedance inside the IGBT module Z_{jc} is normally provided by the manufacturer. In this case, the thermal impedance between junction and case Z_{jc} is obtained from the datasheet [40], as it is shown in Fig. 5 and Table 2. However, the thermal impedance between the case and ambient Z_{ca} is strongly dependent on the design of the cooling system and also on the applied TIM. Thus, their parameters need to be determined either analytically or experimentally. In this case, the parameters of the thermal impedance Z_{ca} are obtained from the experimental result during the cooling phase of the IGBT module following the procedure in [18], [37] (where the influence of heatsink and TIM has been taken into accounted in the thermal impedance). The thermal impedance between the case and ambient Z_{ca} is shown in Fig. 5 and its parameters are provided in Table 2.

TABLE 2 Parameters of the Thermal Impedance Z_{jc} and Z_{ca} [40]

Layer i	1	2	3	4
Thermal resistance $R_{jc,i}$	0.0324	0.1782	0.1728	0.1566
Thermal capacitance $C_{jc,i}$	0.3086	0.1122	0.2894	0.6386
Thermal resistance $R_{ca,i}$	0.0670	0.1737	0.0869	-
Thermal capacitance $C_{ca,i}$	6,157	404.72	37.335	-

TABLE 3 Parameters of the IGBT Lifetime Model [42]

Parameter	Value	Parameter	Value
A	$9.37 \cdot 10^{14}$	β_5	-0.761
β_1	-4.416	β_6	-0.5
β_2	1285	I_B	12.5
β_3	-0.463	V_C	12
β_4	-0.716	D	30

3) LIFETIME MODEL

The wear-out failure of the IGBT due to the thermal stress (e.g., bond-wire lift-off and solder fatigue) can be estimated from the lifetime model (through the cycle counting algorithm). The lifetime estimation procedure for the PV inverter has been comprehensively explained in [27]. In this paper, the lifetime model proposed in [42] is employed, where the number of cycle-to-failure of the IGBT can be calculated as:

$$N_f = A(\Delta T_j)^{\beta_1} \cdot \exp\left(\frac{\beta_2}{T_{j,\min} + 273}\right) \cdot t_{on}^{\beta_3} \cdot I_B^{\beta_4} \cdot V_C^{\beta_5} \cdot D^{\beta_6} \quad (3)$$

where the thermal stress parameters are the thermal cycling amplitude ΔT_j, the minimum junction temperature $T_{j,\min}$, and the cycle period t_{on}. The lifetime model parameters are given in Table 3, where A is the IGBT technology factor (i.e.,

$9.34 \cdot 10^{14}$ for 4th generation IGBT technology), I_{B} is the current per bond foot (i.e., in A), V_{C} is voltage blocking class/100 (i.e., 12 for 1200 V IGBT), and D is the bond wire diameter (i.e., in μm). The remaining coefficients (i.e., $\beta_1, \beta_2, \ldots, \beta_6$) are constant, as discussed in [7], [42]. It should be noted that the main failure mechanism of the lifetime model in (3) is related to the thermo-mechanical stress between the chip and bond-wire and between the solder interconnections, which only takes into account the load duration t_{on} above 1 second. Thus, it is mainly applicable for the thermal stress dynamic induced by the mission profile of the PV inverter (while the thermal stress dynamic at the fundamental output frequency is not considered) [43], [44].

From the lifetime model, it is normally assumed that the contribution of each thermal cycle to the wear-out failure of the IGBT is accumulated linearly and independently following the Miner's rule [10], where the Accumulated Damage AD of the IGBT can be calculated as:

$$AD = \sum_i \frac{n_{\mathrm{i}}}{N_{\mathrm{fi}}} \quad (4)$$

with n_i being the number of cycles at a certain stress level ($T_{\mathrm{j,min}}$, ΔT_{j}, and t_{on}), and N_{fi} being the number of cycles to failure calculated from (3) at that stress condition. The end-of-life of the IGBT is reached when the AD is accumulated to 1, e.g., after a certain period of operation. A comprehensive discussion about the lifetime estimation of PV inverter has been provided in [27].

It should be mentioned that this work mainly focuses on the accuracy of thermal stress modeling, while the accuracy of the lifetime prediction (e.g., time-to-failure) is beyond the scope of this work. However, the lifetime model in (3) and (4) will be used as a quantitative measure of the deviation in the lifetime modeling process introduced by different thermal stress modeling approaches.

C. MISSION PROFILE OPERATION

1) ELECTRICAL LOADING OF INVERTERS

A daily mission profile is applied to the test-bench in order to obtain the thermal stress profile from the experiment. In this case, a relatively high-dynamic mission profile is selected as shown in Fig. 6(a), which occurs during cloudy conditions. In Fig. 6(a), the sampling rate of the mission profile is 1 second/sample (different sampling rates of the mission profile will be considered in the next section). It can be seen from the experimental results that the PV power extraction follows the available power well with the MPPT operation. The fluctuation in the PV power will introduce the high-dynamic thermal stress of the PV inverter, which will also challenge the accuracy of the thermal modeling. Thus, this mission profile is considered as a benchmark case for the model validation in this paper.

2) THERMAL LOADING OF INVERTERS

According to (2), the thermal stress of the PV inverter is contributed by the power losses in the IGBTs (and Diodes) as well

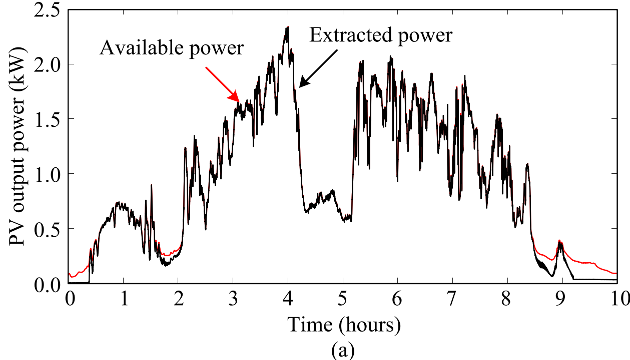

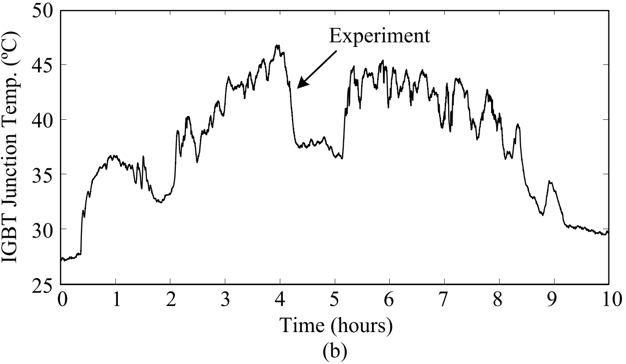

FIGURE 6. Experimental results of the PV inverter test-bench under one-day mission profile operation with cloudy conditions: a) PV power extraction and b) Thermal stress of the IGBT (i.e., junction temperature), where the ambient temperature is $T_{\mathrm{a}} = 25$ °C.

as the ambient temperature variation T_{a}. During the test, the ambient temperature is kept constant at $T_{\mathrm{a}} = 25$ °C, in order to simplify the test infrastructure requirements. The obtained thermal stress of the PV inverter under real mission profile operation is shown in Fig. 6(b). In this case, the sampling rate of the temperature measurement is 1 kHz (with the data acquisition period of 1 second). In this way, several sampling points of the temperature measurement can be obtained for each load change. It should be noted that the experimental test is carried out in real-time, where the testing time is 10 hours (corresponding to the PV inverter loading period during the day). Thus, the test can emulate the thermal loading of the PV inverter under real-field operation and the impact of mission profile dynamics on the thermal stress can clearly be seen.

III. THERMAL STRESS ANALYSIS (EXPERIMENTS)

There are two main factors that influence the dynamics of the thermal stress of the IGBT in PV inverters. One factor is related to the material property of the inverter power stage (e.g., IGBTs and their interface), which is represented by the (transient) thermal impedance. Another factor is due to the load dynamics, which are mainly related to the mission profile resolution (i.e., sampling rate). The impacts of both factors on the accuracy of thermal stress modeling will be demonstrated experimentally and analyzed further in this section.

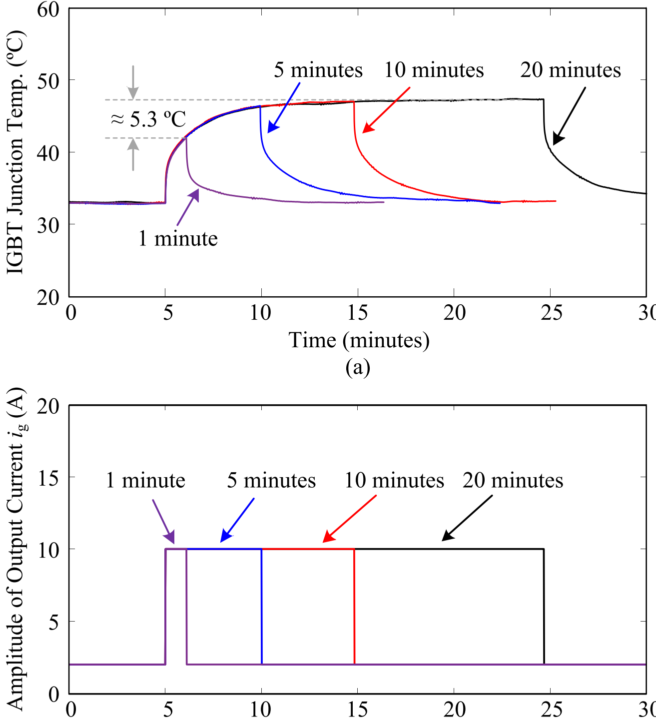

FIGURE 7. **Experimental measurement of PV inverter thermal stress when different load pulse durations (e.g., 1 minute, 5 minutes, 10 minutes, and 20 minutes) are applied to the PV inverter test-bench: a) IGBT junction temperature and b) Amplitude of the inverter output current.**

A. IMPACT OF THERMAL IMPEDANCE TIME-CONSTANT

According to the thermal model in Fig. 4, the thermal impedance network of the power stage in the PV inverter can be divided into two parts: 1) between junction and case of the IGBT Z_{jc} and 2) between case of the IGBT and ambient Z_{ca}. Each thermal impedance network exhibits its own time-constant τ, which separates the transient and steady-state thermal impedance. According to the thermal impedance characteristic in Fig. 5, the time-constant of Z_{jc} is approximately $\tau_{jc} = 1$ second while the time-constant of Z_{ca} is about $\tau_{ca} = 10$ minutes. In this case, the overall thermal dynamic of the power stage is limited by the thermal impedance between the case and ambient Z_{ca}, which reaches the steady-state only after about 10 minutes. This implies that, for a load duration below 10 minutes, the response of the thermal stress (e.g., junction temperature dynamics) will be affected by the transient thermal impedance of both thermal networks Z_{jc} and Z_{ca}.

The impact of the thermal impedance time-constant on the thermal stress dynamic is demonstrated experimentally in Fig. 7, where a load pulse duration of 1 minute, 5 minutes, 10 minutes, and 20 minutes are applied. It can be seen from the results that the final (i.e, peak value) junction temperature is reaching the steady-state for the load duration of 10 minutes and 20 minutes. These results represent the case where a load duration is longer than the time-constant of Z_{ca}. However, the thermal stress dynamics are still in the transient phase when the load duration of 1 minute and 5 minutes are applied. In that case, the temperature difference between the peak value and the steady-state temperature could be higher than 5 °C when the load duration is 1 minute. Therefore, the time-constant of the thermal impedance has a strong impact on the dynamic of the thermal stress, and applying an inappropriate thermal impedance model (e.g., steady-state or dynamic) can be one source of uncertainty in the thermal stress modeling, which will be demonstrated in the next section.

B. IMPACT OF MISSION PROFILE RESOLUTION

In PV applications, the load duration of the inverter is defined by the mission profile dynamics. A fast variation in the solar irradiance is usually induced by passing clouds, as it has been demonstrated in Fig. 6(a). In practice, the long-term mission profile is recorded with a certain sampling rate, referred to as a resolution of the mission profile. In other words, the maximum dynamics of the mission profile (in the thermal stress analysis) is limited by its resolution. Obviously, employing a high resolution (e.g., fast sampling rate) will ensure that the fast dynamics of the real mission profile can be captured, and the representative mission profile will be close to the real-field operation. However, it will also result in a large number of data points for the thermal stress simulation, increasing the computational burden. On the contrary, using a low-resolution mission profile will inevitably introduce a deviation in the mission profile representation, and thereby reduce the accuracy in the thermal stress modeling [45].

In the previous research [46]–[50], a broad range of mission profile resolutions have been applied, typically in the range of 1 second to 15 minutes, since the variation in the PV power is in that time-scale. The thermal stress in Fig. 6(b) which is obtained from the mission profile with a resolution of 1 second per sample is used as a benchmark case (representing the most accurate mission profile dynamics). The mission profiles with the resolution of 1 minute, 5 minutes, and 10 minutes, which are recorded from the same day, are applied to the PV inverter test-bench. The obtained thermal stress profiles are shown in Fig. 8 and compared with the benchmark case. It can be seen from the results in Fig. 8(a) that most of the thermal stress dynamics can still be captured when applying 1-minute resolution mission profile. However, as the mission profile resolution reduces to 10 minutes which is shown in Fig. 8(c), the fast variation in the thermal stress is no longer represented. In Fig. 8(c), mostly the steady-state thermal stress can be observed when a mission profile resolution of 10 minutes is applied. In that case, part of the thermal cycling information related to the small (but fast) junction temperature variation is lost when the mission profile resolution is 10 minutes, and introducing uncertainty in the lifetime estimation [38].

IV. CONVENTIONAL THERMAL MODELING METHODS

In this section, two conventional thermal modeling approaches based on the lumped thermal network will be presented. The advantages and limitations of each thermal model

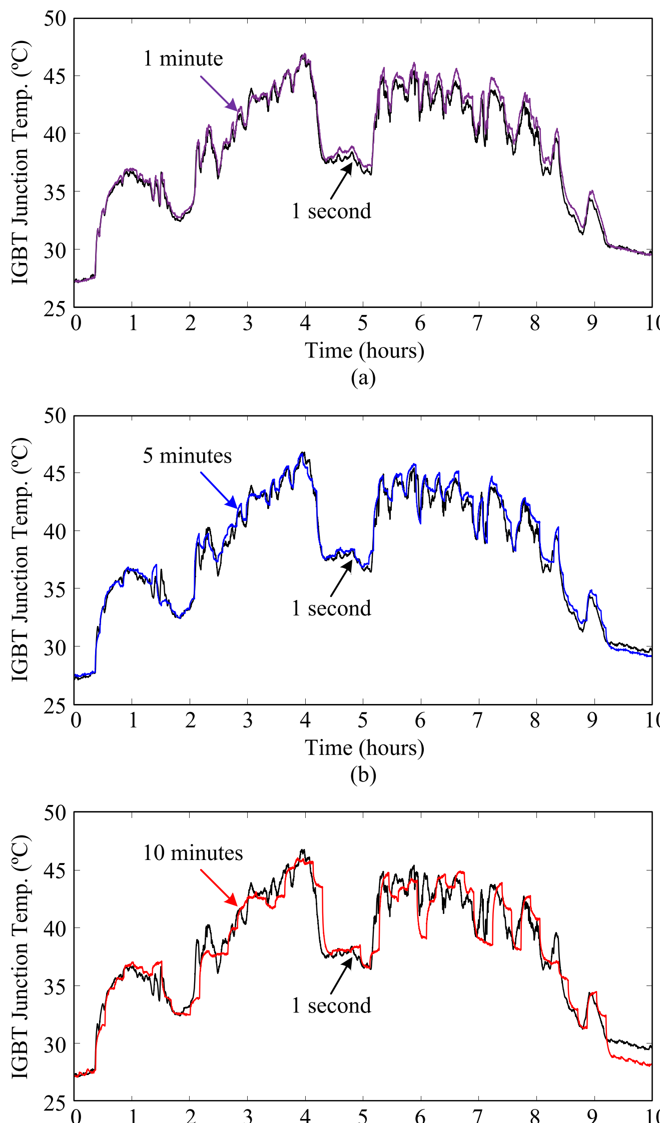

FIGURE 8. Experimental results of the thermal stress of the PV inverter under one-day mission profile with different resolutions of: a) 1 minute, b) 5 minutes, and c) 10 minutes, where the ambient temperature is T_a = 25 °C.

in the thermal stress modeling will be discussed and demonstrated.

A. FULL-ORDER LUMPED THERMAL NETWORK

The most commonly used approach for thermal stress modeling has been previously presented in Fig. 4 [24]–[28]. This model will be referred to as a full-order lumped thermal network, since it includes all transient thermal impedance in the thermal network (e.g., between the junction and case Z_{jc} and between the case and ambient Z_{ca}). The presence of the thermal capacitance makes this thermal model capable of representing the dynamics of thermal stress behavior. However, it also increases the computational burden, especially when the number of order increases, which is the main drawback of this thermal modeling method.

A comparison between the experimental and simulation results with a full-order thermal model is carried out by applying a step-load with different load durations. According to the results in Fig. 9, the full-order thermal model can capture the dynamic of the thermal stress well regardless of the load duration. It can also be noticed that the final junction temperature is not reaching the steady-state when the load duration of 1 minute and 5 minutes are applied as shown in Fig. 9(a) and 9(b). This demonstrates the case where the load dynamics are below the time-constant of the thermal impedance Z_{ca}, which is $\tau_{ca} = 10$ minutes.

B. STEADY-STATE LUMPED THERMAL NETWORK

Another thermal modeling approach, which is commonly used for long-term thermal stress analysis, is the steady-state thermal model [29]–[31]. In this approach, the thermal network is represented only by the thermal resistance, as shown in Fig. 10, while the thermal capacitance, which mainly influences the transient dynamics, is neglected. On one hand, this thermal model is very simple and resource-effective in terms of implementation. It also provides a good accuracy of the thermal stress estimation during steady-state. On the other hand, the transient behavior of the thermal stress cannot be captured with this steady-state thermal model, since there is no time-constant of the thermal impedance, due to the absence of the thermal capacitance.

The thermal stress profiles obtained from the steady-state thermal model under different load durations are also shown in Fig. 9. It can be seen from the results in Fig. 9(a) and 9(b) that there is a certain deviation in the thermal stress estimation, e.g., maximum junction temperature, when the load duration is below 10 minutes, which is the time-constant of the thermal impedance Z_{ca}. However, the steady-state model can estimate the junction temperature (e.g., final value) quite accurately when the load duration is above the time-constant of the thermal impedance Z_{ca} (which is closer to the steady-state), as it is shown in Fig. 9(c) and 9(d).

V. PROPOSED REDUCED-ORDER THERMAL MODELING

Based on the previous results, the steady-state thermal model cannot fully capture the dynamics of thermal stress while the full-order thermal model demands more computational efforts. To address this issue, a thermal model simplification method is proposed in this section.

A. THERMAL MODEL SIMPLIFICATION

It has been demonstrated in the previous section that both the time-constant of the thermal impedance and the load dynamics influence the dynamics of the thermal stress of the PV inverter. The load dynamics are then in turn influenced by the mission profile resolution. Thus, by knowing a correlation between the time-constant of the thermal impedance and the applied mission profile resolution, a model simplification can

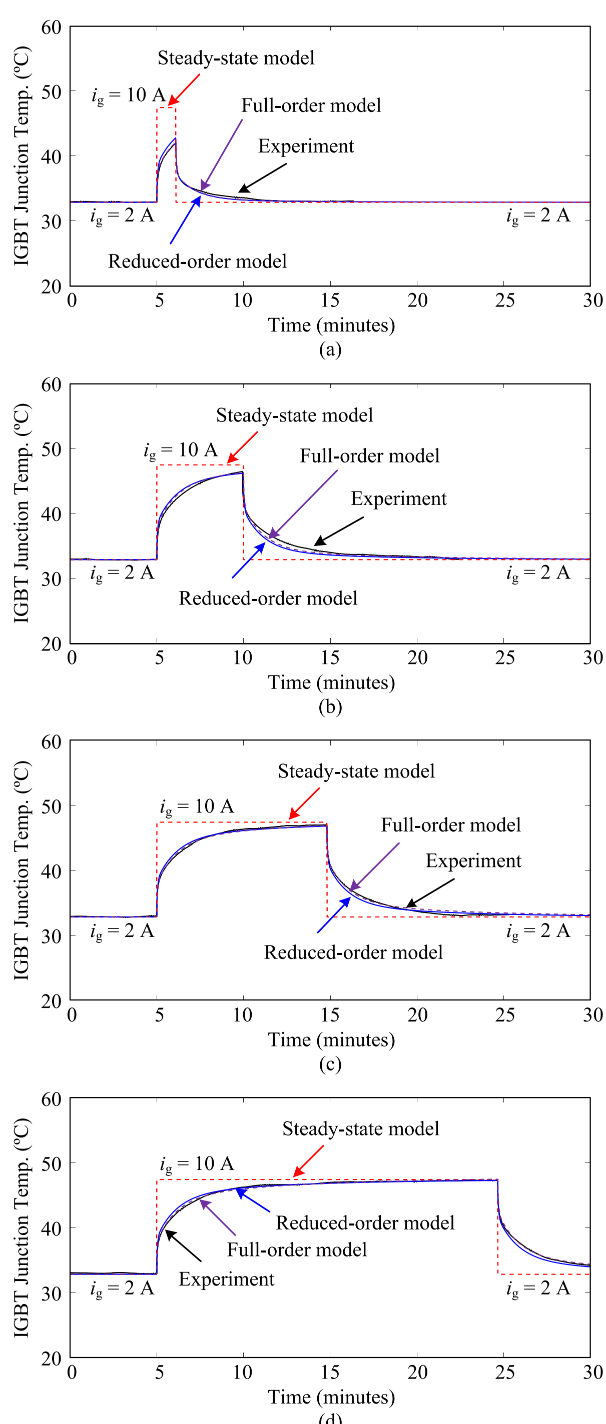

FIGURE 9. Simulation and experimental results of thermal stress obtained from the full-order, steady-state, and reduced-order thermal models when the load dynamics (i.e., load durations) of: a) 1 minute, b) 5 minutes, c) 10 minutes, and d) 20 minutes, are applied.

be applied to the thermal network and reduce the computational burden while maintaining the model accuracy.

According to the thermal impedance characteristic in Fig. 5, the two thermal impedance networks Z_{jc} and Z_{ca} are responsible for different time-scales. For instance, the transient

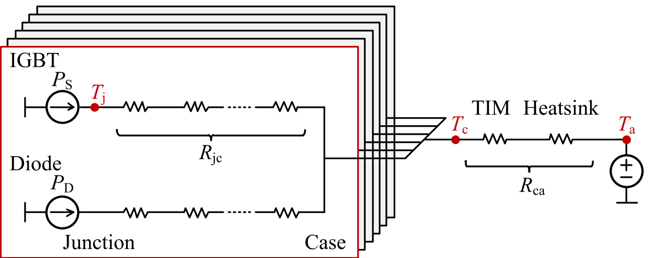

FIGURE 10. Thermal model of three-phase IGBT module in PV inverter based on steady-state lumped thermal network.

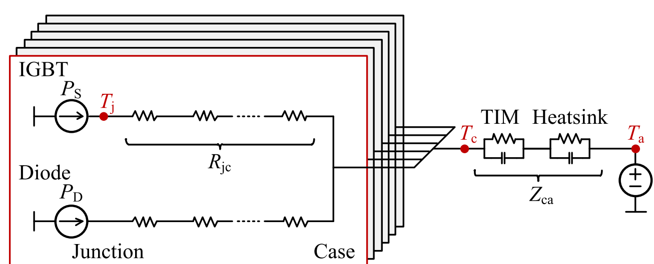

FIGURE 11. Thermal model of three-phase IGBT module in PV inverter based on reduced-order lumped thermal network.

thermal impedance between the junction and case Z_{jc} only applies to a load duration below 1 second. If the load duration is above 1 second, the temperature variation between junction and case of the IGBT T_{jc} can be considered as being in steady-state. A similar consideration is applied for the thermal impedance between the case and ambient Z_{ca}. However, in this case, the time-constant of the thermal impedance is much longer than Z_{jc}, where the steady-state thermal impedance can be considered only if the load duration is longer than a couple of minutes (e.g., 10 minutes). Accordingly, part of the transient thermal impedance network can be simplified to the thermal resistance, if the load dynamics are above the time-constant of its thermal impedance.

B. REDUCED-ORDER LUMPED THERMAL NETWORK

In order to apply this method to the thermal model of the PV inverter, the dynamics of the mission profile needs to be considered. In PV applications, the mission profile dynamics are in the range of a few seconds to minutes, considering the dynamics of solar irradiance. It that case, it can be assumed that the temperature variation between the junction and case is in steady-state due to its short time-constant. Thus, the thermal network between junction and case Z_{jc} can be simplified to a thermal resistance R_{jc}. On the contrary, the time-constant of the thermal impedance between the case and ambient Z_{ca} lies within the mission profile dynamics in PV applications. Thus, the transient thermal impedance needs to be considered in order to estimate the temperature variation between the case and ambient. The reduced-order thermal model based on this model order reduction approach is shown in Fig. 11 and a block diagram for implementation is illustrated in Fig. 12.

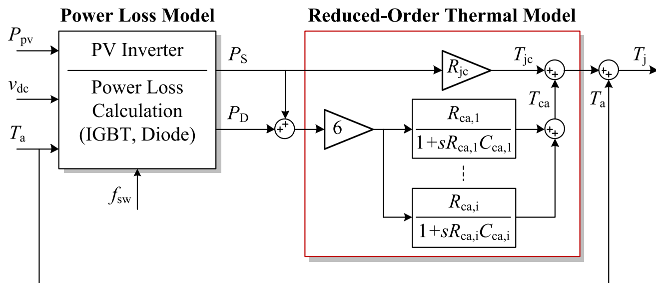

FIGURE 12. A simplified diagram of the reduced-order thermal model applied to three-phase IGBT module in PV inverter.

A comparison between experiments and simulations with the reduced-order thermal model is carried out with different load durations, as it is shown in Fig. 9. Compared to the conventional thermal model approaches, the reduced-order thermal model can capture the thermal stress during the transient, especially, when the load duration is below the thermal time constant, similar to the full-order thermal model. This can be seen from the junction temperature estimation when the load duration of 1 minute and 5 minutes are applied, as it is shown in Fig. 9(a) and 9(b).

VI. BENCHMARKING OF THERMAL STRESS MODELING

In this section, a case study of a one-day mission profile for PV inverter is applied to the full-order, the steady-state, and the reduced-order thermal models. The mission profile resolutions of 1 second, 1 minute, 5 minutes, and 10 minutes are considered, and the performance of the thermal models are benchmarked in terms of model accuracy (e.g., thermal stress and thermal cycling) and computational efficiency.

A. THERMAL STRESS ANALYSIS

1) FULL-ORDER THERMAL MODEL

The simulation and experimental results of the thermal stress when applying the full-order thermal model are shown in Fig. 13. Since all the transient thermal impedances are considered in the full-order thermal model, the dynamics of the thermal stress can be estimated accurately even during the fast variation as it is shown in Fig. 13(a). At the same time, the thermal stress under a slow variation of mission profile dynamics in Fig. 13(d) can also be accurately estimated.

2) STEADY-STATE THERMAL MODEL

Unlike the full-order thermal model, a certain deviation in the thermal stress estimation can be observed in Fig. 14 where the steady-state thermal model is applied. It can be clearly seen from the results in Fig. 14(a)-(c) that the steady-state thermal model introduces a considerable deviation in the thermal stress estimation when the mission profile resolution is below 10 minutes. This confirms that the assumption of the steady-state thermal model is no longer valid when the load duration is below the time-constant of the thermal impedance. On the other hand, the steady-state thermal model can effectively

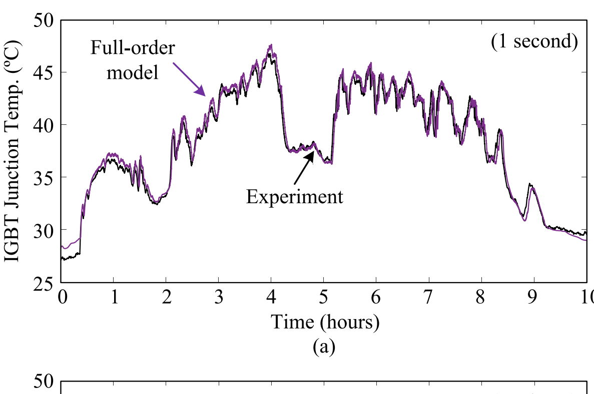

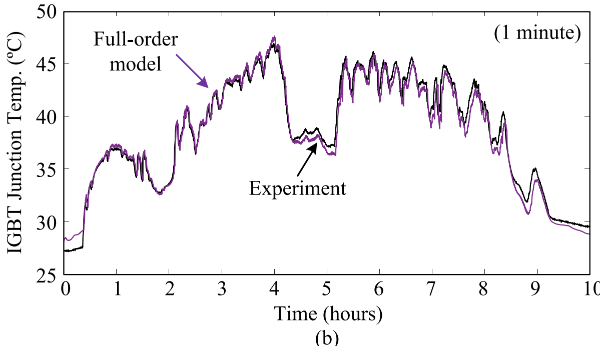

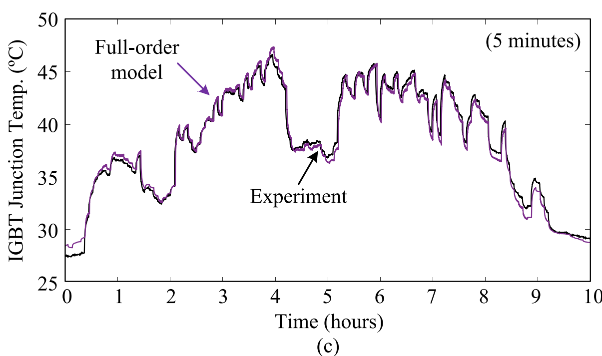

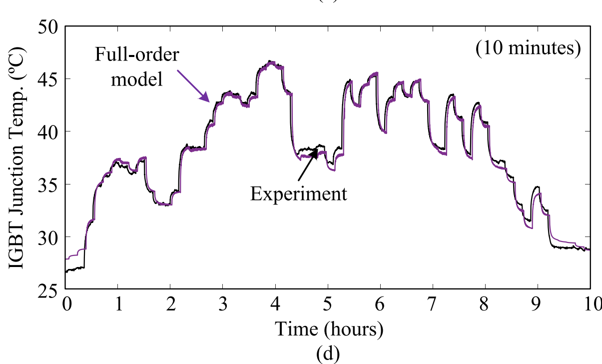

FIGURE 13. Simulation and experimental results of thermal stress obtained from the full-order thermal model when the mission profile resolution of: a) 1 second, b) 1 minute, c) 5 minutes, and d) 10 minutes, are applied, where the ambient temperature is T_a = 25 °C.

estimate the thermal stress of the PV inverter when the load duration is above the time-constant of the thermal impedance. This can be seen by a significant reduction in the deviation between the simulations and experiments once the mission profile resolution above 10 minutes is applied in Fig. 14(d).

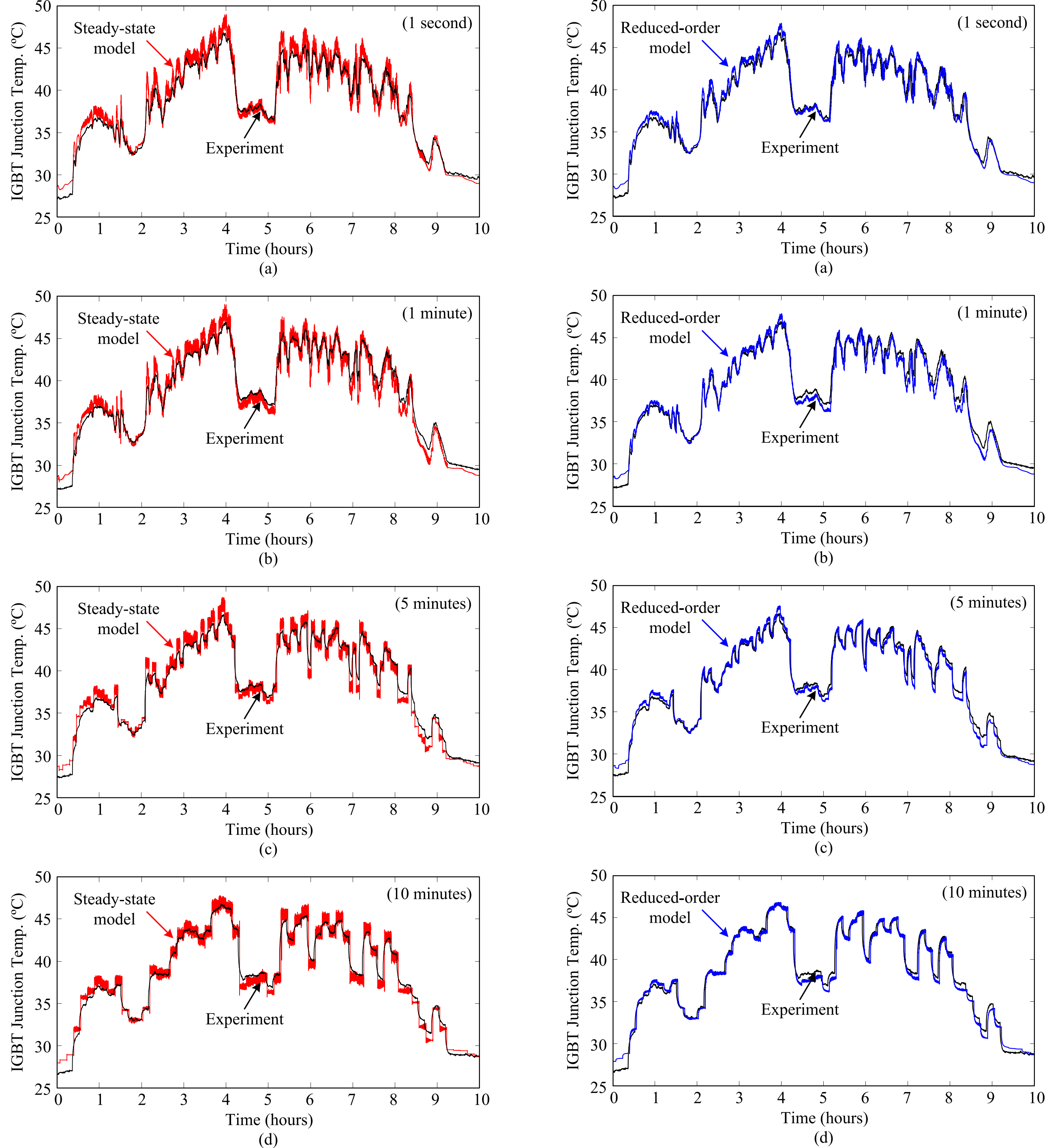

FIGURE 14. **Simulation and experimental results of thermal stress obtained from the steady-state thermal model when the mission profile resolution of: a) 1 second, b) 1 minute, c) 5 minutes, and d) 10 minutes, are applied, where the ambient temperature is $T_a = 25\ ^{\circ}$C.**

FIGURE 15. **Simulation and experimental results of thermal stress obtained from the reduced-order thermal model when the mission profile resolution of: a) 1 second, b) 1 minute, c) 5 minutes, and d) 10 minutes, are applied, where the ambient temperature is $T_a = 25\ ^{\circ}$C.**

3) REDUCED-ORDER THERMAL MODEL

The same mission profiles are applied to the reduced-order thermal model, and the estimated thermal stress profiles are shown in Fig. 15. It can be seen from the results that the estimation of the thermal stress dynamics improves significantly with the reduced-order thermal model, e.g., compared to the steady-state thermal model. In this case, most of the fast variation in the thermal stress can be captured even when the high resolution of mission profile (e.g., 1 second) is applied, as it is shown in Fig. 15(a). Therefore, the dynamics of thermal stress estimation is similar to the case where the full-order

TABLE 4 **Average Deviation between Simulation and Experimental Results of Thermal Stress**

Mission Profile Resolution	Thermal Model		
	Full-Order	Steady-State	Reduced-Order
1 second	1.50 %	2.08 %	1.58 %
1 minute	1.51 %	2.03 %	1.59 %
5 minutes	1.33 %	1.94 %	1.41 %
10 minutes	0.83 %	1.78 %	0.98 %

thermal model is applied. As the mission profile resolution decreases (e.g., from 1 second to 10 minutes), the accuracy of the thermal stress estimation is improved, similar to the other thermal models. Therefore, the reduced-order thermal model is capable of estimating the thermal stress dynamics under a wide-range of mission profile resolutions.

B. MODELING ACCURACY FOR JUNCTION TEMPERATURE ESTIMATION

The accuracy of the thermal stress modeling can be evaluated from the average deviation of the junction temperature estimation. In this case, the average deviation ε between the junction temperature profile obtained from the simulation $T_{\mathrm{j,sim}}$ and the experiment $T_{\mathrm{j,exp}}$ (under the same mission profile resolution) can be calculated as:

$$\varepsilon = \frac{|T_{\mathrm{j,exp}} - T_{\mathrm{j,sim}}|}{T_{\mathrm{j,exp}}} \cdot 100 \tag{5}$$

The average deviation of the junction temperature estimation when applying the different thermal models under various mission profile resolutions is summarized in Table 4. In general, it can be seen that the estimation deviation decreases as the mission profile resolution decreases, which is similar to the observation in the time-domain waveforms of the thermal stress profiles. On the other hand, the accuracy of the thermal stress estimation can be improved by employing either the full-order or the reduced-order thermal models, where the deviation from the two models are comparable. For all mission profile resolutions that are being considered, the maximum average deviation for the junction temperature estimation is 2.08%, which is the case when applying the 1-second mission profile resolution to the steady-state thermal model. This deviation indicates the required design margin due to the uncertainty from the thermal stress modeling.

C. MODELING ACCURACY FOR THERMAL CYCLING ESTIMATION

The accuracy of the thermal cycling estimation when applying different thermal models is also evaluated by applying the estimated thermal stress profile to the lifetime model of the IGBT in (3) together with a cycle counting algorithm. Then, the damage *AD* during one-day operation is accumulated based on Miner's rule in (4), which has been discussed in Section II. The calculated *AD* during one-day operation with different thermal modeling approaches are summarized in Table 5, and the estimation deviation is calculated by comparing the *AD*

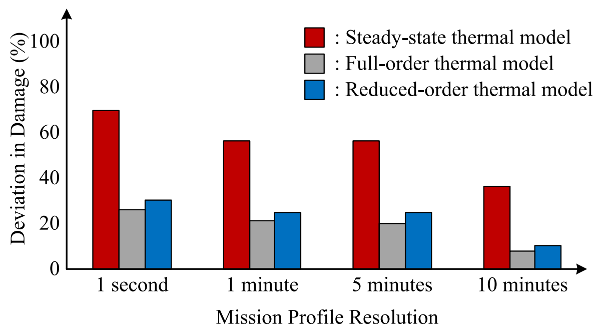

FIGURE 16. **Deviation (in percentage) in the accumulated damage between the experimental and simulation results when applying full-order, steady-state, and reduced-order thermal models for different mission profile resolutions.**

obtained from the simulated thermal stress profile against the *AD* obtained from the experimental thermal stress under the same mission profile resolution. In general, the deviation between the damage calculated from experiments and simulations decreases when the mission profile resolution is reduced, e.g., to 10 minutes. This is coherent with the fact that the thermal stress variation becomes more and more steady-state and thereby the estimation of the thermal stress by all the thermal models becomes more accurate when the dynamic of the mission profile decreases. In contrast, a large deviation in the *AD* estimation can be introduced under a highly dynamic mission profile condition. In that case, the maximum deviation in the *AD* estimation can be as high as 69% when a 1-second mission profile resolution is applied to the steady-state thermal model. However, the deviation in the thermal cycling estimation, and thereby *AD*, can be reduced by selecting a suitable thermal model. Compared to the steady-state thermal model, the deviation between the experimental and simulation results is reduced significantly (e.g., more than a factor of two) with the full-order and the reduced-order thermal models, especially, when the mission profile resolution is below the time-constant of the thermal impedance (e.g., 10 minutes). This is mainly due to the improvement in the transient thermal stress estimation of both thermal models. In that case, the maximum deviations in the *AD* estimation are 26% and 30% for the full-order and the reduced-order thermal models, respectively, which is the case when the 1-second mission profile resolution is considered. A comparison between different thermal models is illustrated in Fig. 16.

D. COMPUTATIONAL EFFICIENCY

Computational efficiency is another important aspect for thermal model selection, especially when considering a long-term analysis. In general, there is a trade-off between the model accuracy and computational-burden. To evaluate this aspect, the required simulation time for different thermal models has been measured when applying a one-day mission profile. The simulation has been carried out in MATLAB/Simulink software with Intel Core i7, 1.80 GHz processor computer platform. The simulation of each thermal modeling approach

TABLE 5 Accumulated Damage of the IGBT When Applying the Full-Order, Steady-State, and Reduced-Order Thermal Models

Mission Profile	Experiment	Full-Order Thermal Model		Steady-State Thermal Model		Reduced-Order Thermal Model	
Resolution	Damage	Damage	Deviation (%)	Damage	Deviation (%)	Damage	Deviation (%)
1 second	$3.46 \cdot 10^{-7}$	$4.35 \cdot 10^{-7}$	26 %	$5.85 \cdot 10^{-7}$	69 %	$4.52 \cdot 10^{-7}$	30 %
1 minute	$3.60 \cdot 10^{-7}$	$4.36 \cdot 10^{-7}$	21 %	$5.62 \cdot 10^{-7}$	56 %	$4.50 \cdot 10^{-7}$	25 %
5 minutes	$3.68 \cdot 10^{-7}$	$4.42 \cdot 10^{-7}$	20 %	$5.75 \cdot 10^{-7}$	56 %	$4.60 \cdot 10^{-7}$	25 %
10 minutes	$4.31 \cdot 10^{-7}$	$4.64 \cdot 10^{-7}$	8 %	$5.85 \cdot 10^{-7}$	36 %	$4.75 \cdot 10^{-7}$	10 %

Note: the deviation is calculated with respect to the experimental result under the same mission profile resolution.

TABLE 6 Required Simulation Time of Thermal Models for One-Day Thermal Stress Analysis

Required Simulation	Thermal Model		
Time	Full-Order	Steady-State	Reduced-Order
Mean μ	2.487 s	0.770 s	1.076 s
Standard Deviation σ	0.316 s	0.095 s	0.122 s

has been repeated multiple times (e.g., 1000 times) in order to obtain a statistical value of the computational efficiency. The results are summarized in Table 6, where it can be seen that the steady-state thermal model requires minimum simulation time compared to the other thermal models. In contrast, the full-order thermal model requires the longest simulation time, which is three times longer than that of the steady-state model. This high computational burden is mainly introduced by a large number of *RC* elements in the lumped thermal model. Therefore, the proposed reduced-order thermal model, which minimizes the number of *RC* elements between the junction and case in the lumped thermal model, can effectively reduce the computational burden by more than a factor of two compared to the full-order thermal model. Accordingly, the required simulation time of the reduced-order thermal model becomes comparable with the steady-state thermal model, indicating a significant improvement in the computational efficiency.

VII. CONCLUSION

In this paper, a method to simplify the thermal model for long-term thermal stress modeling has been proposed for the power devices in PV inverters. The simplification of the thermal model is based on the correlation between the thermal impedance characteristic and the mission profile dynamics, which has been analyzed experimentally with a PV inverter test-bench. In the reduced-order thermal model, the transient behavior of the thermal impedance network (i.e., thermal capacitance) is partially neglected (i.e., between the junction and case of the IGBT module) due to the fact that its time-constant is much shorter than the load dynamics in the PV applications. By doing so, the dynamic of the transient thermal stress can still be captured, while the computational burden of the thermal model is reduced significantly.

A comprehensive evaluation of the accuracy of the proposed reduced-order thermal models has been carried out and compared with the conventional thermal models (i.e., full-order and steady-state thermal models) as well as the experiments under various operating conditions. Based on the evaluation results, the reduced-order thermal model offers a similar thermal stress modeling accuracy as the full-order thermal model. Compared with the experimental results, the maximum deviation in the average junction temperature and the thermal cycling estimation is 1.59% and 30% when applying the reduced-order thermal model. On the other hand, the computational burden of the reduced-order thermal model is reduced by more than a factor of two compared to the full-order thermal model, thanks to the reduced number of *RC* elements in the lumped thermal network. Therefore, the proposed reduced-order thermal model is a very efficient method for the long-term thermal stress modeling for PV inverters.

REFERENCES

[1] P. Hacke *et al.*, "A status review of photovoltaic power conversion equipment reliability, safety, and quality assurance protocols," *Renewable Sustain. Energy Rev.*, vol. 82, pp. 1097–1112, 2018.
[2] Enphase Energy. Reliability - Enphase Energy. Online. [Online]. Available: https://enphase.com/en-au/enphase-advantage/reliability
[3] SMA, "Sunny boy/sunny tripower temperature derating." [Online]. Available: https://files.sma.de/dl/7418/Temp-Derating-TI-en-15.pdf
[4] N. R. Sorensen *et al.*, "Thermal study of inverter components," *IEEE J. Photovolt.*, vol. 3, no. 2, pp. 807–813, Apr. 2013.
[5] H. Wang, M. Liserre, and F. Blaabjerg, "Toward reliable power electronics: Challenges, design tools, and opportunities," *IEEE Ind. Electron. Mag.*, vol. 7, no. 2, pp. 17–26, Jun. 2013.
[6] *Appl. Note 5SYA 2093-00, Therm. design and temperature ratings IGBT modules*, ABB. [Online]. Available: http://library.e.abb.com/
[7] A. Wintrich, U. Nicolai, W. Tursky, and T. Reimann, *Appl. manual power semiconductors. Semikron international GmbH*, 2015.
[8] H. Wang *et al.*, "Transitioning to physics-of-failure as a reliability driver in power electronics," *IEEE J. Emerg. Sel. Topics Power Electron.*, vol. 2, no. 1, pp. 97–114, Mar. 2014.
[9] A. T. Bryant, P. A. Mawby, P. R. Palmer, E. Santi, and J. L. Hudgins, "Exploration of power device reliability using compact device models and fast electrothermal simulation," *IEEE Trans. Ind. App.*, vol. 44, no. 3, pp. 894–903, May 2008.
[10] H. Huang and P. A. Mawby, "A lifetime estimation technique for voltage source inverters," *IEEE Trans. Power Electron.*, vol. 28, no. 8, pp. 4113–4119, Aug. 2013.
[11] K. Ma, H. Wang, and F. Blaabjerg, "New approaches to reliability assessment: Using physics-of-failure for prediction and design in power electronics systems," *IEEE Power Electron. Mag.*, vol. 3, no. 4, pp. 28–41, Dec. 2016.
[12] S. Yang, A. Bryant, P. Mawby, D. Xiang, L. Ran, and P. Tavner, "An industry-based survey of reliability in power electronic converters," *IEEE Trans. Ind. App.*, vol. 47, no. 3, pp. 1441–1451, May 2011.
[13] J. Falck, C. Felgemacher, A. Rojko, M. Liserre, and P. Zacharias, "Reliability of power electronic systems: An industry perspective," *IEEE Ind. Electron. Mag.*, vol. 12, no. 2, pp. 24–35, Jun. 2018.

[14] M. Andresen, K. Ma, G. Buticchi, J. Falck, F. Blaabjerg, and M. Liserre, “Junction temperature control for more reliable power electronics,” *IEEE Trans. Power Electron.*, vol. 33, no. 1, pp. 765–776, Jan. 2018.

[15] M. Musallam, C. Yin, C. Bailey, and M. Johnson, “Mission profile-based reliability design and real-time life consumption estimation in power electronics,” *IEEE Trans. Power Electron.*, vol. 30, no. 5, pp. 2601–2613, May 2015.

[16] V. Blasko, R. Lukaszewski, and R. Sladky, “On line thermal model and thermal management strategy of a three phase voltage source inverter,” in *Proc. IEEE IAS Annu. Meeting*, vol. 2, pp. 1423–1431, Oct. 1999.

[17] Chan-Su Yun, P. Malberti, M. Ciappa, and W. Fichtner, “Thermal component model for electrothermal analysis of IGBT module systems,” *IEEE Trans. Adv. Packag.*, vol. 24, no. 3, pp. 401–406, Aug. 2001.

[18] Z. Luo, H. Ahn, and M. A. E. Nokali, “A thermal model for insulated gate bipolar transistor module,” *IEEE Trans. Power Electron.*, vol. 19, no. 4, pp. 902–907, Jul. 2004.

[19] M. Musallam and C. M. Johnson, “Real-time compact thermal models for health management of power electronics,” *IEEE Trans. Power Electron.*, vol. 25, no. 6, pp. 1416–1425, Jun. 2010.

[20] B. Du, J. L. Hudgins, E. Santi, A. T. Bryant, P. R. Palmer, and H. A. Mantooth, “Transient electrothermal simulation of power semiconductor devices,” *IEEE Trans. Power Electron.*, vol. 25, no. 1, pp. 237–248, Jan. 2010.

[21] C. Batard, N. Ginot, and J. Antonios, “Lumped dynamic electrothermal model of IGBT module of inverters,” *IEEE Trans. Compon. Packag. Manuf. Technol.*, vol. 5, no. 3, pp. 355–364, Mar. 2015.

[22] K. Ma, A. S. Bahman, S. Beczkowski, and F. Blaabjerg, “Complete loss and thermal model of power semiconductors including device rating information,” *IEEE Trans. Power Electron.*, vol. 30, no. 5, pp. 2556–2569, May 2015.

[23] C. H. van der Broeck, L. A. Ruppert, A. Hinz, M. Conrad, and R. W. De Doncker, “Spatial electro-thermal modeling and simulation of power electronic modules,” *IEEE Trans. Ind. App.*, vol. 54, no. 1, pp. 404–415, Jan. 2018.

[24] N. Sintamarean, H. Wang, F. Blaabjerg, and P. P. Rimmen, “A design tool to study the impact of mission-profile on the reliability of SiC-based PV-inverter devices,” *Microelectron. Reliab.*, vol. 54, no. 9, pp. 1655–1660, 2014.

[25] P. D. Reigosa, H. Wang, Y. Yang, and F. Blaabjerg, “Prediction of bond wire fatigue of IGBTs in a PV inverter under a long-term operation,” *IEEE Trans. Power Electron.*, vol. 31, no. 10, pp. 7171–7182, Oct. 2016.

[26] C. Felgemacher, S. Araujo, C. Noeding, P. Zacharias, A. Ehrlich, and M. Schidleja, “Evaluation of cycling stress imposed on IGBT modules in PV central inverters in sunbelt regions,” in *Proc. CIPS*, pp. 1–6, Mar. 2016.

[27] A. Sangwongwanich, Y. Yang, D. Sera, and F. Blaabjerg, “Lifetime evaluation of grid-connected PV inverters considering panel degradation rates and installation sites,” *IEEE Trans. Power Electron.*, vol. 33, no. 2, pp. 1225–2361, Feb. 2018.

[28] R. k. Gatla, W. Chen, G. Zhu, J. V. Wang, and S. S. Kshatri, “Lifetime comparison of IGBT modules in grid-connected multilevel PV inverters considering mission profile,” in *Proc. of. ICPE 2019 - ECCE Asia*, pp. 2764–2769, May 2019.

[29] S. E. De Len-Aldaco, H. Calleja, F. Chan, and H. R. Jimnez-Grajales, “Effect of the mission profile on the reliability of a power converter aimed at photovoltaic applications - a case study,” *IEEE Trans. Power Electron.*, vol. 28, no. 6, pp. 2998–3007, Jun. 2013.

[30] F. Chan and H. Calleja, “Reliability estimation of three single-phase topologies in grid-connected PV systems,” *IEEE Trans. Ind. Electron.*, vol. 58, no. 7, pp. 2683–2689, Jul. 2011.

[31] E. Koutroulis and F. Blaabjerg, “Design optimization of transformerless grid-connected PV inverters including reliability,” *IEEE Trans. Power Electron.*, vol. 28, no. 1, pp. 325–335, Jan. 2013.

[32] C. Qian *et al.*, “Thermal management on IGBT power electronic devices and modules,” *IEEE Access*, vol. 6, pp. 12 868–12 884, 2018.

[33] Y. Zhang, H. Wang, Z. Wang, and F. Blaabjerg, “Simplified multi-time scale thermal model considering thermal coupling in IGBT modules,” in *Proc. of. APEC*, pp. 319–324, Mar. 2019.

[34] K. Ma and F. Blaabjerg, “Multi-timescale modelling for the loading behaviours of power electronics converter,” in *Proc. of. ECCE*, pp. 5749–5756, Sep. 2015.

[35] K. Ma, M. Liserre, F. Blaabjerg, and T. Kerekes, “Thermal loading and lifetime estimation for power device considering mission profiles in wind power converter,” *IEEE Trans. Power Electron.*, vol. 30, no. 2, pp. 590–602, Feb. 2015.

[36] K. Ma, N. He, M. Liserre, and F. Blaabjerg, “Frequency-domain thermal modeling and characterization of power semiconductor devices,” *IEEE Trans. Power Electron.*, vol. 31, no. 10, pp. 7183–7193, Oct. 2016.

[37] *Transient Thermal Measurements and Thermal Equivalent Circuit Models*, Infineon Technologies AG, 2018, rev. 1.1.

[38] A. Sangwongwanich, H. Wang, and F. Blaabjerg, “Impact of mission profile dynamics on accuracy of thermal stress modeling in PV inverters,” in *Proc. ECCE*, pp. 1–7, Oct. 2020.

[39] F. Blaabjerg, R. Teodorescu, M. Liserre, and A.V. Timbus, “Overview of control and grid synchronization for distributed power generation systems,” *IEEE Trans. Ind. Electron.*, vol. 53, no. 5, pp. 1398–1409, Oct. 2006.

[40] *FS50R12KT4_B15*, Infineon Technologies AG, 2009, rev. 3.0.

[41] *IGBT Power Losses Calculation Using Data-Sheet Parameters*, Infineon Technologies AG, 01 2009, rev. 1.1.

[42] R. Bayerer, T. Herrmann, T. Licht, J. Lutz, and M. Feller, “Model for power cycling lifetime of IGBT modules - various factors influencing lifetime,” in *Proc. of. CIPS*, pp. 1–6, Mar. 2008.

[43] G. Zeng, R. Alvarez, C. Knzel, and J. Lutz, “Power cycling results of high power IGBT modules close to 50 Hz heating process,” in *Proc. of. EPE ’19 ECCE Eur.*, pp. 1–10, 2019.

[44] J. Lutz, C. Schwabe, G. Zeng, and L. Hein, “Validity of power cycling lifetime models for modules and extension to low temperature swings,” in *Proc. of. EPE ’20 ECCE Eur.*, pp. 1–9, 2020.

[45] A. Sangwongwanich, D. Zhou, E. Liivik, and F. Blaabjerg, “Mission profile resolution impacts on the thermal stress and reliability of power devices in PV inverters,” *Microelectron. Reliab.*, vol. 88-90, pp. 1003–1007, 2018.

[46] J. M. Lenz, H. C. Sartori, and J. R. Pinheiro, “Mission profile characterization of PV systems for the specification of power converter design requirements,” *Sol. Energy*, vol. 157, pp. 263–276, 2017.

[47] M. Andresen, G. Buticchi, and M. Liserre, “Thermal stress analysis and MPPT optimization of photovoltaic systems,” *IEEE Trans. Ind. Electron.*, vol. 63, no. 8, pp. 4889–4898, Aug. 2016.

[48] M. Dbeiss, Y. Avenas, and H. Zara, “Comparison of the electro-thermal constraints on SiC MOSFET and Si IGBT power modules in photovoltaic DC/AC inverters,” *Microelectron. Rel.*, vol. 78, pp. 65–71, 2017.

[49] A. Anurag, Y. Yang, and F. Blaabjerg, “Thermal performance and reliability analysis of single-phase PV inverters with reactive power injection outside feed-in operating hours,” *IEEE Trans. Emerg. Sel. Topics Power Electron.*, vol. 3, no. 4, pp. 870–880, Dec. 2015.

[50] S. Harb and R. S. Balog, “Reliability of candidate photovoltaic module integrated-inverter (PV-MII) topologies’a usage model approach,” *IEEE Trans. Power Electron.*, vol. 28, no. 6, pp. 3019–3027, Jun. 2013.